Hemodynamic Influence on Smooth Muscle Cell Kinetics and Phenotype During Early Vein Graft Adaptation

Benjamin Klein,[1,2] Anthony Destephens,[3] Leanne Dumeny,[1,2] Qiongyao Hu,[1,2] Yong He,[1,2] Kerri O'Malley,[1,2] Zhihua Jiang,[1,2] Roger Tran-Son-Tay,[3,4] and Scott Berceli[1,2,4]

[1]Malcom Randall VA Medical Center, Gainesville, FL, USA; [2]Department of Surgery, University of Florida, Box 100128, Gainesville, FL 32610-0128, USA; [3]Department of Mechanical and Aerospace Engineering, University of Florida, Gainesville, FL, USA; and [4]Department of Biomedical Engineering, University of Florida, Gainesville, FL, USA

Associate Editor Scott I. Simon oversaw the review of this article.

Abstract—Pathologic vascular adaptation following local injury is the primary driver for accelerated intimal hyperplasia and an occlusive phenotype. Smooth muscle cell (SMC) proliferation within the wall, and migration into the developing intima, is a major component of this remodeling response. The primary objective in the current study was to investigate the effect of the local biomechanical forces on early vein graft adaptation, specifically focusing on the spatial and temporal response of SMC proliferation and conversion from a contractile to synthetic architecture. Taking advantage of the differential adaptation that occurs during exposure to divergent flow environments, vein grafts were implanted in rabbits to create two distinct flow environments and harvested at times ranging from 2 h to 28 days. Using an algorithm for the virtual reconstruction of unfixed, histologic specimens, immunohistochemical tracking of DNA synthesis, and high-throughput transcriptional analysis, the spatial and temporal changes in graft morphology, cell proliferation, and SMC phenotype were catalogued. Notable findings include a burst of cell proliferation at 7 days post-implantation, which was significantly augmented by exposure to a reduced flow environment. Compared to the adjacent media, proliferation rates were 3-fold greater in the intima, and a specific spatial distribution of these proliferating cells was identified, with a major peak in the subendothelial region and a second peak centering on the internal elastic lamina. Genomic markers of a contractile SMC phenotype were reduced as early as 2 h post-implantation and reached a nadir at 7 days. Network analysis of upstream regulatory pathways identified GATA6 and KLF5 as important transcription factors that regulate this shift in SMC phenotype.

INTRODUCTION

The intermediate to long-term failure rate of vein grafts remains an obstacle in the treatment of vascular disease.[6] Undermining progress towards a solution is the incomplete understanding of the complex biological mechanisms of vein graft remodeling that leads to clinical failure. Changes in the rate of smooth muscle cell (SMC) proliferation within the media and intima are thought to be contributors to this remodeling process.[10,22,27,32]

A focus of our laboratory has been a systems-based understanding of vein graft failure.[4,9,14,15] Critical to this effort is the synergistic use of high-fidelity data sets and theoretical models, which combine to elevate our insight into this problem. As such, cataloguing the overall effects and interactions among the various biologic adaptation processes is fundamental to this effort, and data sets with high spatial and temporal resolution are required for validation and refinement of these integrated approaches.

Within this context, our primary objective in the current study was to investigate the effect of the local biomechanical forces on early vein graft adaptation, specifically focusing on the dynamic response of SMC proliferation and their conversion from a contractile to synthetic architecture. To accomplish this, we have implemented a novel algorithm for the in silico reconstruction of vein graft architecture from histologic sections and coupled this with high-throughput transcriptional analysis of the regulatory pathways that modulate SMC phenotype.

Address correspondence to Scott Berceli, Department of Surgery, University of Florida, Box 100128, Gainesville, FL 32610-0128, USA. Electronic mail: bercesa@surgery.ufl.edu
Benjamin Klein and Anthony Destephens have contributed equally to this work.

644

MATERIALS AND METHODS

Animal Model

Our laboratory has a long-standing interest in understanding the pathobiology related to altered flow dynamics in the vascular system, and we utilized our established rabbit model to create unique phenotypes of successful and failed vein graft adaptation. Using a polymeric cuff to create the anastomoses, New Zealand White Rabbits (3.0–3.5 kg) underwent bilateral carotid artery interposition grafting with jugular vein.[17] Briefly, the external jugular veins were harvested (3.0 cm in length) for creation of an inter-position graft into the common carotid artery. Grafts were constructed using an anastomotic cuff, fashioned from a 4-French introducer sheath (Terumo Medical Corporation, Elkton, MD). Proximal and distal ends of the jugular vein were passed through cuffs, everted, and fixed using 8-0 silk. The carotid artery lumen was then exposed using a 2.0–2.5 cm arteriotomy and the cuffed vein inserted into the proximal and distal ends. A second 8-0 silk was used to secure the artery around the intraluminal cuff. Finally, the intervening segment of the carotid artery between the cuffs was excised, to provide a uniform degree of vein graft extension.

Differential flow states between the right and left vein grafts were accomplished *via* unilateral ligation of the internal carotid artery and three of the four primary branches of the external carotid artery (Fig. 1). Flow reduction on the side of the ligation (low flow graft) and contralateral compensation (high flow graft) resulted in an immediate 10-fold difference in mean wall shear stress between the left and right grafts. Rabbit jugular veins placed in the absence of distal ligation demonstrated a flow rate intermediate to the high and low flow grafts and was used as a comparator.

Vein grafts were harvested at 2 h ($n = 29$), 1 day ($n = 23$), 3 days ($n = 26$), 7 days ($n = 34$), 14 days ($n = 27$), and 28 days ($n = 30$) after implantation. One hour prior to harvest, rabbits received an intramuscular injection of bromodeoxyuridine (BrdU; 50 mg/kg), a nucleotide analogue of thymidine with a unique immunologic epitope to facilitate tracking of proliferative cells. Intraluminal pressure and graft flow rate were measured at the time of graft harvest using a pressure-transducing catheter (Millar, model TCB-600), and an ultrasonic flow meter (Transonic Systems, Inc., Ithaca, NY, model T106, probe 2SB), respectively. Using a Womersley harmonic decomposition scheme previously published by our group,[8] dynamic wall shear stress was calculated at each graft harvest time and flow condition. The mean circumferential wall stress ($T_{\theta\theta}$) at each time and flow condition was estimated using a modification of Laplace's Law ($T_{\theta\theta} = Pr/h$), where P is the mean intraluminal graft pressure, r is the lumen radius, and h is the wall thickness.

At the time of graft harvest, *in vivo* vein graft geometry was determined using a high-resolution ultrasound imaging system (Vevo 2100, with a MS-250, 21 MHz transducer, VisualSonics, Inc., Ontario, Canada). With the system providing a native resolution of 20 μm, B-mode ultrasound images were obtained in a transverse orientation at two locations (proximal and distal) in the graft, which corresponded to the sites of tissue acquisition for histologic processing. Computer aided morphometry was performed to measure the cross-sectional area of the lumen and outer graft wall. Assuming a circular geometry, area measurements were used to calculate the average, *in vivo* graft diameter (at the EEL) and intima/media thickness for each graft.

To facilitate the simultaneous analysis of both transcriptional profiling and histomorphometric analysis, harvested grafts were freshly excised and flushed with 0.9% saline to remove blood. The anastomotic cuffs and the adjacent 2-mm segments were discarded. The proximal and distal portions of the remaining graft were immersed in 10% formalin for 24 h, dehydrated through graded alcohols, and paraffin embedded. Care was taken to mount the cut surface of each specimen in a plane perpendicular to the paraffin block surface.

This study was approved by the Institutional Animal Care and Use Committee and conforms to the Guide for the Care and Use of Laboratory Animals (NIH Publication, Revised 2011). Additional details of the vein graft model have been previously described.[17]

Immunohistochemistry and Histology

Actively proliferating cells undergoing cell cycle S-phase incorporate BrdU into their newly transcribed DNA in place of thymidine. The BrdU epitope was identified using a high-affinity antibody to provide nuclear-specific staining over the activated cell (Fig. 2). Histologic cross-sections (5 μm thickness) were processed using an Invitrogen BrdU staining kit according to manufacturer's recommendations. A series of histomicrographs (×40 magnifications, 5–10 images per section) were collected and re-assembled to provide a single high-resolution image of the entire graft cross-section.
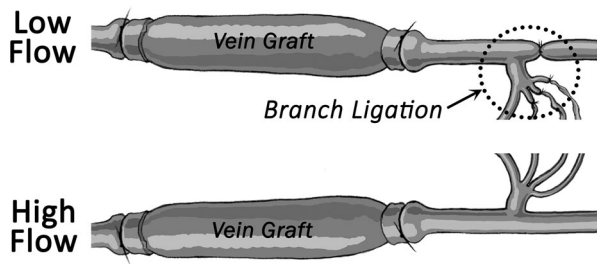
FIGURE 1. Bilateral vein graft with distal branch ligation model. The most inferior branch of the external carotid served as the only outflow for the low flow graft on the ligated side, resulting in two distinct flow regimes.

In Silico Geometric Reconstruction of the In Vivo Graft Geometry

An overview of the reconstruction algorithm and the steps taken to approximate an *in vivo* geometry are illustrated in Fig. 3 and described below.

(1) Image processing software (AxioVision version 4.8, Zeiss) was used to identify the centroid of each stained nucleus, and the Cartesian coordinates of the centroid tabulated. No histologic counterstain was employed to facilitate automation and minimize artifact. Birefringence of the specimen was sufficient to visualize the lumen surface and the histologic changes between the various layers of the graft wall. The border between the intima and media (internal elastic lamina, IEL) was determined by the transition from a disorganized SMC pattern in the intima to the uniform circumferential organization of these cells in the media. The border between the media and adventitia (external elastic lamina, EEL) was defined by the transition from a tight cellular/matrix network in the media to the loose collagen distribution in the adventitia. The lumen, IEL, and EEL were manually traced and their locations recorded using the previously defined coordinate system. Co-registration with an adjacent, Masson's stained histologic section was used to confirm the locations of these borders. Stained nuclei with a position overlying the lumen boundary were considered adherent circulating cells and were removed from all subsequent calculations.

(2) After the position of each boundary line on the vein graft cross-section was digitized, the distances between the lumen and IEL and then the IEL and EEL were calculated using a nearest neighbor method. Specifically, the algorithm sequentially analyzed each point along the luminal contour to identify the closest neighboring point on the IEL, with an analogous

approach being used to define the minimum IEL-EEL distances. The line connecting the lumen-IEL (or IEL-EEL) and passing through the centroid of each positively stained nucleus was identified and used to define the relative distance of the cell from each of these boundaries during the reconstruction process.

Approximating the *in vivo* graft to be an isotropic material with a uniform intraluminal pressure, the pressurized graft was assumed to adopt a circular lumen geometry. The perimeter of the dehydrated lumen was determined and used to calculate the radius of a circle, which served as the starting point for the reconstruction. Once the lumen was circularized, the inter-point distances between the lines of each boundary were used to reconstruct the IEL and EEL positions. The coordinates of each nuclear centroid were also redefined using a similar inter-point distance algorithm. Minimum distances from the closet point on the lumen and IEL were determined, and used to define both the normalized depth and circumferential location of stained nuclei within the intima. Similarly, the closest points on the IEL and EEL were used to define the normalized depth and circumferential location of nuclei within the media.

(3) During histologic fixation and embedding, dehydration of the tissue results in shrinkage that is manifested as a reduction in the cross-sectional area of the graft wall.[31] A series of validation studies, with microscopic imaging at multiple points during histologic processing, was used to define a post-processing to pre-processing ratio for vascular tissue of 0.75. Using this ratio, the medial and intimal areas were increased by radially expanding each point on the IEL and EEL through an iterative process until each layer had a 25% increase in area.

(4) To reconstruct the final *in vivo* geometry, ultrasound images obtained at the time of graft harvest were used to define the *in vivo* diameter under pressurized (arterial) conditions. Using individualized data obtained for each graft, a new circular lumen was determined. Assuming the intima and media are incompressible and their areas remain constant, the *in vivo* dimensions of the circularized IEL and EEL are provided by the following expressions:

$$R_{\text{IEL}} = \sqrt{\frac{A_{\text{intima}}}{\pi} + R_{\text{lumen}}^2}$$

$$R_{\text{EEL}} = \sqrt{\frac{A_{\text{media}}}{\pi} + R_{\text{IEL}}^2}$$

where R_{lumen} is the experimentally determined *in vivo* lumen radius; A_{intima} and A_{media} are the estimated compartment areas determined after virtual rehydration (step 3); and R_{IEL} and R_{EEL} are the estimated *in vivo* radii of the IEL and EEL, respectively. During this final "re-pressurization" step, the centroid of the stained nucleus was migrated inward or outward in a radial direction, to maintain the fractional distance between the lumen and IEL (or IEL–EEL) determined after Step 3. To illustrate the spectrum of geometries encountered in the current analysis, Fig. 4 displays the original, histologic sections and final, *in vivo* renderings of six specimens included in our data set.

Determining Proliferative Cell Densities

The spatial arrangement of the BrdU-stained nuclei within each section was quantified both as a function of the actual distance from the lumen (or IEL) and the normalized depth within the intima or media. To determine normalized depth, the area between the lumen and IEL (intima) or IEL and EEL (media) was divided into ten sections of uniform thickness, and each cell was categorized as belonging to one of these ten sections. The proliferative density of each section was then calculated by dividing the number of stained nuclei by the total area of that section.
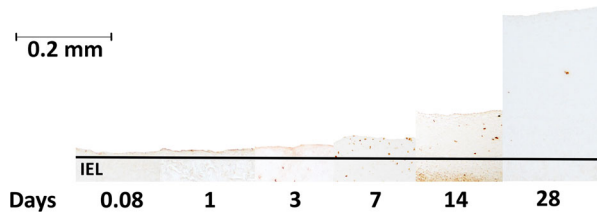

FIGURE 2. Representative sections stained for BrdU, a marker of DNA synthesis and cell proliferation. This arrangement illustrates the progressive phenotypic change experienced by implanted vein grafts over time.
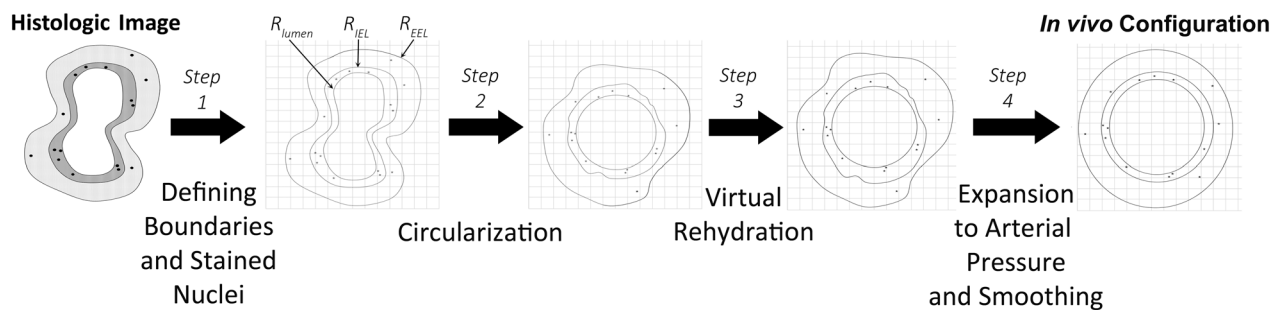
Transcriptional Regulation of SMC Phenotype

For tracking the dynamic changes in SMC phenotype that are associated with the kinetics of cell proliferation, mRNA content of genes specific for a contractile SMC were evaluated. Vein samples, stripped of the adventitia and endothelium, were homogenized in Buffer RLT (Qiagen, Valencia, CA) using a Miltenyi Gentle MACS dissociator followed by Qiashredder for lysis (Qiagen). RNA isolation was performed using RNeasy MiniKit (Qiagen), and quality confirmed using an Agilent Bioanalyzer. cDNA was generated using Ovation Pico WT kit (NuGEN, San Carlos, CA) and labeled using GeneChip WT Terminal Labeling (Affymetrix, Santa Clara, CA). Samples were hybridized to a proprietary rabbit array (Affymetrix). SMC markers trangelin (TAGLN, SM-22), SMC myosin heavy chain (MYH11) and α-actin (ACTA) were selected as genes representative of conversion from contractile to sythetic phenotype and analyzed for their dependence on time and flow conditions.[23,25] Ingenuity Pathway Analysis (IPA) (Ingenuity, Redwood City, CA) was employed to identify upstream genes with a direct connection to TAGLN, MYH11, or ACTA. This list was cross-referenced to the rabbit array annotated gene list to identify overlapping genes, and this final gene set was analyzed for both temporal expression patterns following vein graft placement and divergent expression profiles between the high and low flow conditions.

Statistical Analysis

Global differences among dependent variables were evaluated with a one-, two-, or three-way ANOVA, as dictated by the dimensionality of the data, and a Holm-Sidak *post hoc* analysis was used to identify differences between individual groups (SigmaStat, San Jose, CA). The relationship between the ultrasound measured and reconstruction-algorithm estimated wall

FIGURE 3. Virtual reconstruction of the *in vivo* graft geometry and location of proliferating cells is obtained *via* a four-step algorithm: (1) automated identification of stained nuclei and manual tracing of the compartment boundaries; (2) circularization of the lumen surface; (3) virtual rehydration to account for the volume loss secondary to processing with isopropyl alcohol and paraffin embedding; (4) compartmental smoothing and expansion of the lumen to account for arterial pressurization.
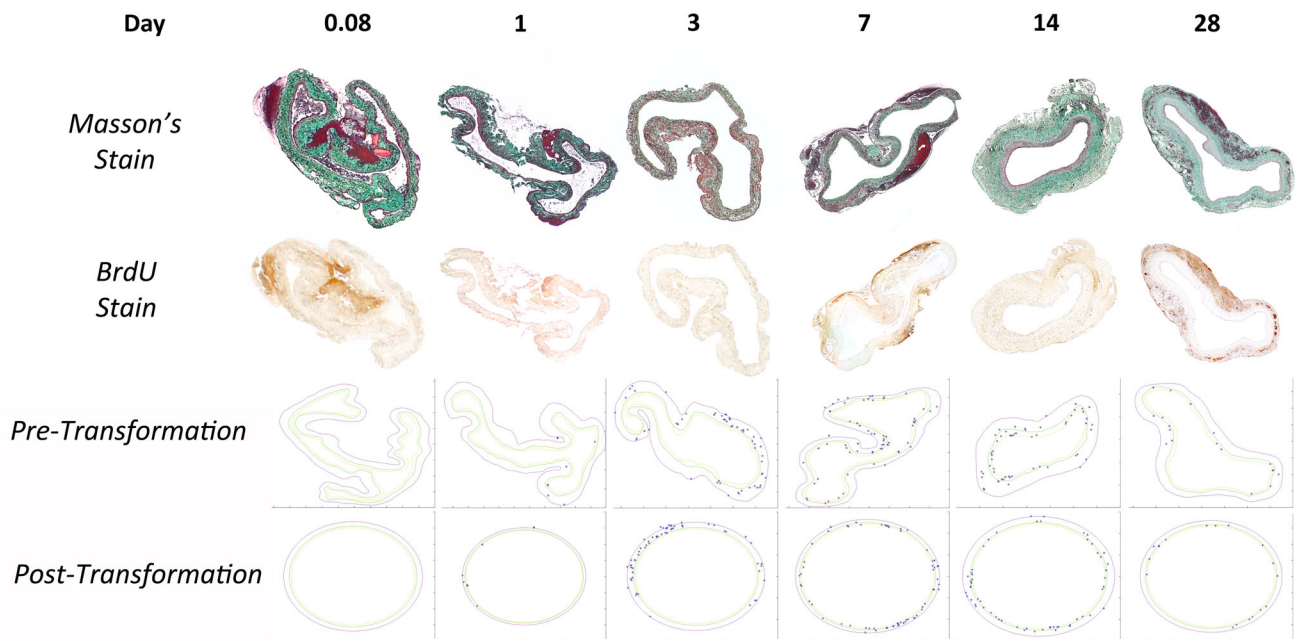
FIGURE 4. Representative Masson's and BrdU stained sections with accompanying reconstructions for vein grafts harvested at times ranging from 2 h to 28 days. Note the change from highly convoluted geometry to a more circularized structure between 7 and 14 days, which corresponds to the rapid expansion of the intima.

thickness and lumen diameter was evaluated with a Pearson Correlation Coefficient. Data are expressed as mean $\pm$ standard error of the mean (SEM), and $p > .05$ was considered to be non-significant (NS).

RESULTS

Quantification of the Hemodynamic Environment

Bilateral carotid vein grafting with unilateral, partial ligation resulted in an immediate 8-fold difference in flow rate (Day 0.08: High: 40.2 ± 5.4 ml/min; Low: 4.9 ± 1.3 ml/min), which persisted through the duration of the experiment (Day 28: High: 38.3 ± 5.6 ml/min; Low: 2.1 ± 0.9 ml/min). Comparing low and high flow grafts, these flow differences translated into a 5- to 10-fold difference in mean and a 3- to 5-fold difference in peak (maximum) wall shear stress at each of the time points investigated (Table 1). In contrast, non-ligated vein grafts served as a baseline comparator, with an average flow rate of 35.0 ± 8.1 ml/min and mean wall shear stress of 10.3 ± 0.5 dynes/cm^2.

Implantation of the vein graft induces thickening of the wall and expansion of the lumen. As such, coincident with the change in shear forces are modifications in the intramural wall tensile forces. Increases in wall thickness dominate the extent of luminal expansion. From implantation to Day 28, this results in a reduction in circumferential wall stress ranging from 47% to 69%, depending on the flow condition (Table 1).

Morphologic Changes in Response to Altered Hemodynamic Forces

Intimal growth within the vein grafts was observed to be both time and flow dependent ($p < .001$ time, $p < .001$ flow; two-way ANOVA; Fig. 5a). Most notable was the effect of the hemodynamic environment, where exposure to a low flow condition induced a rapid and pronounced growth in the intima. These flow dependent differences were most apparent several weeks following implantation. By Day 14, the average intimal area of the low flow environment grafts was significantly higher than those from the high and intermediate flow grafts (High: 0.26 ± 0.03 mm^2, Intermediate: 0.41 ± 0.16 mm^2, Low: 0.58 ± 0.29 mm^2; $p = .009$ low vs. intermediate, $p < .001$ low vs. high flow; *post hoc* analysis). This trend was more pronounced by Day 28, at which point the low flow grafts demonstrated a 2-fold greater area when compared to the high flow grafts (High: 0.36 ± 0.07 mm^2, Intermediate: 0.45 ± 0.08 mm^2, Low: 0.78 ± 0.32 mm^2; $p < .001$ low vs. intermediate, $p < .001$ low vs. high flow; *post hoc* analysis).

Although more tempered, the medial compartment also exhibited time dependent growth, while no hemodynamic impact on medial cross-sectional area was observed ($p < .001$ time, $p =$ NS flow; two-way ANOVA; Fig. 5b).

Evaluation of the accuracy of the reconstruction algorithm was performed through comparison of the ultrasound measured outer graft diameter and wall thickness against the predicted geometry for grafts

TABLE 1. Wall shear stress and circumferential wall stress of implanted vein grafts following exposure to various flow conditions.

	Wall shear stress (dynes/cm²)						Mean circumferential wall stress (× 10⁶ dynes/cm²)		
	High flow		Low flow		Intermediate flow				
Day	Peak	Mean	Peak	Mean	Peak	Mean	High flow	Low flow	Intermediate flow
0.08	23.4 ± 2.4	12.0 ± 1.2	4.4 ± 0.7	1.2 ± 0.2	21.0 ± 2.9	9.0 ± 1.2	1.55 ± 0.34	1.44 ± 0.27	1.66 ± 0.28
1	20.0 ± 1.5	10.3 ± 0.8	4.3 ± 0.6	1.3 ± 0.2	29.1 ± 2.2	12.5 ± 1.0	1.81 ± 0.26	1.43 ± 0.29	1.41 ± 0.21
3	26.0 ± 4.3	13.4 ± 2.2	5.2 ± 1.1	1.5 ± 0.3	31.7 ± 4.7	13.7 ± 2.2	1.33 ± 0.28	1.34 ± 0.32	1.13 ± 0.32
7	29.6 ± 3.3	15.2 ± 1.7	9.3 ± 2.6	2.7 ± 0.8	24.8 ± 0.7	10.7 ± 0.3	0.59 ± 0.17	0.70 ± 0.20	0.81 ± 0.18
14	21.1 ± 4.8	10.9 ± 2.5	6.4 ± 2.3	1.9 ± 0.7	23.3 ± 2.1	10.0 ± 0.9	0.54 ± 0.24	0.88 ± 0.33	0.60 ± 0.14
28	16.0 ± 2.0	8.2 ± 1.0	3.9 ± 1.4	1.1 ± 0.4	13.6 ± 0.5	5.9 ± 0.2	0.48 ± 0.10	0.76 ± 0.12	0.82 ± 0.11

Data: Average ± SEM.

harvested at 28 days following implantation (Fig. 6). The measured and predicted graft diameter (at the EEL) were highly correlated ($r = 0.94$, $p < .0001$), with no systematic differences resulting from the imposed flow condition. Although demonstrating more variation than the graft geometry, the ultrasound measured intima/media thickness was also strongly correlated with predicted values obtained from the reconstruction ($r = 0.64$, $p < .0001$). Increased inaccuracies were most apparent in samples exposed to low flow conditions, likely resulting from non-uniformities in the intimal hyperplastic process and the inability of the reconstruction algorithm to accurately model these circumferential variations in wall thickness.

Cell Proliferation—Effect of Time, Flow, and Position

The proliferative density, averaged over the entire intima, was observed to be dependent on the time of implantation ($p < .001$; two-way ANOVA; Fig. 7a), increasing from the 2 h baseline, peaking at Day 7, and returning back to near baseline by Day 28 (Day 0.08: 0.6 ± 0.6 cells/mm²; Day 7: 106 ± 4 cells/mm²; Day 28: 10.8 ± 2.8 cells/mm²). In addition, during the period of maximum intimal proliferation (Day 7), there was significant dependence on the hemodynamic condition ($p < .001$), where grafts from the low flow condition displayed the highest intimal proliferative density of any group examined (High: 76.5 ± 5.9 cells/mm², Intermediate: 81.2 ± 6.4 cells/mm², Low: 161 ± 7 cells/mm²; $p < .001$ low vs. intermediate, $p < .001$ low vs. high flow; *post hoc* analysis).

Total medial proliferative density was also found to be time dependent ($p < .001$; two-way ANOVA; Fig. 7b), peaking at Day 3 (80.4 ± 15.5 cells/mm²). Similar to the observed changes in medial area, proliferative density within this compartment was independent of the imposed hemodynamics ($p = $ NS; two-way ANOVA).

To accommodate differences in graft morphology, a normalization approach was utilized. Each compartment was divided into ten sections of equal thickness, with zero representing the lumen or IEL, in the intima or media respectively (Fig. 8, Supplemental Fig. 1). The normalized, position-dependent analysis demonstrated the proliferative density within the intima to be highly dependent on the depth within both the intimal and medial compartments ($p < .001$; three-way ANOVA). Focusing on the peak time for cell replication (Day 7), the proliferative density in the intima was significantly elevated in the region adjacent to the IEL ($p < .001$, IEL Position 1.0 vs. all other positions; *post hoc* analysis).

Removing the normalization scheme, and examining proliferation as a function of the actual depth into the tissue, demonstrated a similar pattern, with augmented cell replication on both sides of the IEL. Supplemental Fig. 2 displays physical cell depth in the intima referenced to the lumen, and Supplemental Fig. 3 displays medial cell distances referenced to the IEL.

Evolution of SMC Phenotypes

Gene expression profiles for known markers of SMC differentiation (TAGLN, MYH11, and ACTA) were investigated to define the time and flow dependent shifts in the contractile phenotype (Fig. 9). Compared to mRNA content at the time of initial vein harvest, all three markers demonstrated reduced expression as early as the 2 h post-implantation time point. Significant time dependence was observed in the expression of all markers (TAGLN: $p < .001$, MYH11: $p < .001$, ACTA: $p = .016$, time; two-way ANOVA), with a reduction that ranged from 60 to 90% at the Day 7 nadir. Also notable was the hemodynamic influence on two of the three markers (TAGLN: $p < .001$, MYH11: $p < .035$, flow; two-way ANOVA) with high flow
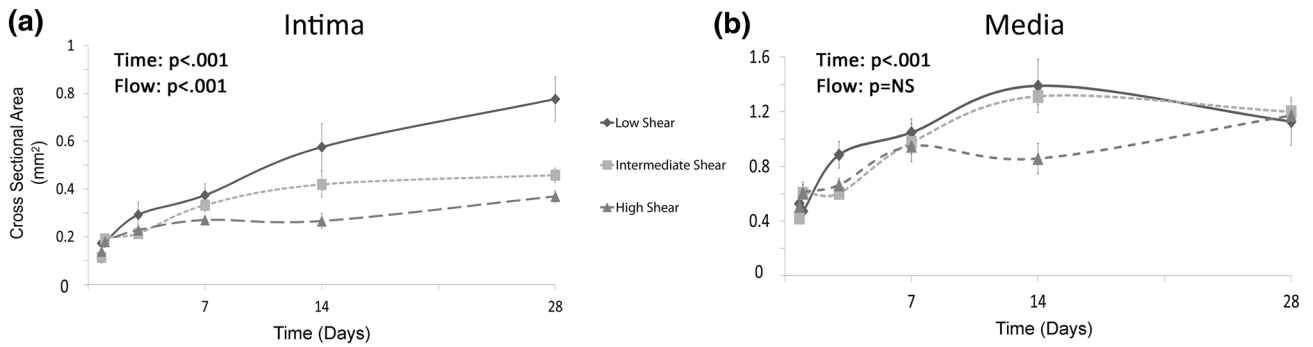
FIGURE 5. Changes in intimal and medial cross-sectional area following graft implantation. (a) Significant time and flow dependent growth of the intima was observed ($p < .001$ time, $p < .001$ flow). Most notable was the difference in the intimal area of the low flow vs. high and intermediate flow grafts, several weeks after implantation (Day 14: $p = .009$ low vs. intermediate, $p < .001$ low vs. high flow; Day 28: $p < .001$ low vs. intermediate, $p < .001$ low vs. high flow). (b) In contrast, the medial area demonstrates modest time dependent growth but is relatively unaffected by modulation of the flow. ($p < .001$ time, p = NS flow).
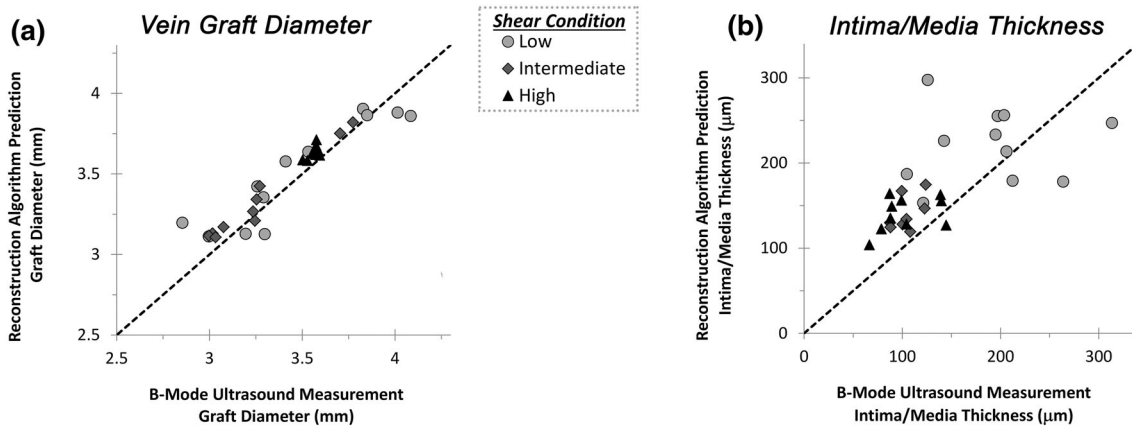

FIGURE 6. Examination of the algorithm predicted vs. ultrasound measured architecture of vein grafts harvested 28 days following implantation. (a) A high correlation in the measured and predicted graft outer diameter was observed ($r = 0.94$, $p < .0001$). (b) Although demonstrating some increased variation in low flow grafts, the ultrasound measured intima/media thickness was also strongly correlated with predicted values obtained from the reconstruction ($r = 0.64$, $p < .0001$).
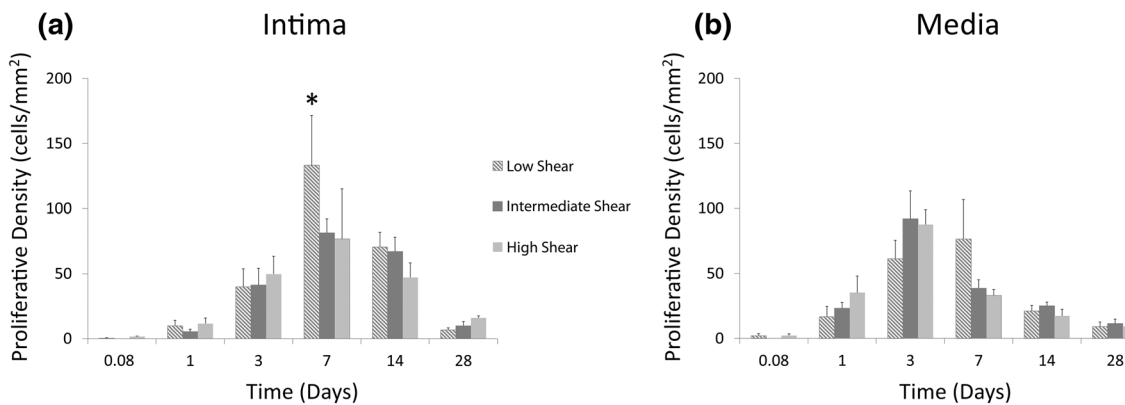

FIGURE 7. Significant time-dependent differences in proliferative density within both the intima and media are observed ($p < .001$). (a) In the intima, overall proliferation initially peaks at Day 7 and returns to baseline quiescent levels by Day 28. Consistent with the subsequent difference in intimal growth rates, enhanced proliferation was observed in the low flow grafts 1 week following implantation (Day 7: *$p < .001$ low vs. intermediate, $p < .001$ low vs. high flow). (b) In contrast, the medial compartment demonstrated a Day 3 peak in proliferative density, which was independent of the imposed flow condition.

conditions inducing an increase in mRNA expression most prominently 2–4 weeks after implantation.

A functional network analysis was performed to identify those upstream genes that have a direct regulatory impact on TAGLN, MYH11, and ACTA expression. Forty-two regulators that mapped to the custom Affymetrix rabbit array were identified (Supplemental Table 1). A complex pattern of augmentation and inhibition was observed, with changes ranging from a 275% increase to 92% reduction in gene expression (Supplemental Fig. 4). A rapid increase in Kruppel-Like Factor 5 (KLF5), within 2 h of graft implantation, appears to initiate the reduction in TAGLN transcription. This is followed closely by a Day 1 increases in Macrophage Myristoylated Alanine-Rich C Kinase Substrate (MARCKSL-1), Ribosomal Protein S7 (RPS7), and transcription factor GATA6, which appear to be primary drivers for downregulating ACTA and MYH11 transcription.

DISCUSSION

Based on morphologic and mechanistic studies, vascular adaptation to altered shear stress encompasses two distinct processes: intimal hyperplasia and wall (inward/outward) remodeling.[22] Intimal hyperplasia is characterized by migration of SMC into the intima with proliferation and deposition of extracellular matrix, resulting in narrowing of the arterial lumen.[23] In contrast, remodeling is characterized by preservation or loss of lumen area through re-organization of the cellular and extracellular components within the media. The acute transposition of a vein segment from a low pressure/flow environment to the high pressure/flow arterial system leads to significant structural changes within the wall, characterized by a burst of SMC proliferation, the deposition of collagen and proteoglycans, and a net increase in both intimal and medial thickness.[21,32] Local wall shearing forces have been postulated as a major regulator of these events.

While this shift in SMC biology from a contractile to synthetic phenotype has been well characterized in cultures systems and idealized vascular injury models, this conversion has not been systematically examined in a clinically relevant model such as vein bypass grafting. Among the few studies to examine these early changes in vein grafts utilized immunohistochemistry and transmission electron microscopy to examine a collection of autopsy specimens obtained in the initial days to weeks after failed coronary artery bypass grafting.[19] Their analysis demonstrated that soon after grafting, the circular layer of the media is severely damaged, resulting in a loss of SMC, with the remaining SMC in this layer show a change toward the synthetic pheno-type. Unique to the current study is delineation of the time course for downregulation of TAGLN, MYH11, and ACTA transcription and the regulator elements that control these changes. GATA6 and KLF5 are zinc finger transcription factors with well-established roles in regulating cell cycle activity and the differentiation state of various cell types throughout the body.[23,25] Not previously described are the potential roles that MARCKSL-1 and RPS7 may play in shepherding this SMC conversion to a synthetic phenotype.

The current study confirms the previously published results of our laboratory[8,17] and others[7,21,26] stating that the blood flow rate is a significant regulator of both intimal growth and cell proliferation. Unique to this manuscript is the observation that cell proliferation following vein graft implantation occurs most prominently within the intimal and medial regions adjacent to IEL. This observation, coupled with the finding that growth of the media after 7 days is relatively modest, suggests that cell proliferation in the media and migration into the intima is an important component of the hyperplastic vein graft response. Although a kinetic analysis of cell death and extracellular matrix metabolism would be required to fully validate this hypothesis, such a conclusion would have profound importance in the development of therapeutic approaches and delivery vectors to mitigate pathologic vein graft remodeling.

This analysis of cell proliferation kinetics following vein graft implantation was undertaken as part of a multiscale modeling effort to identify the optimum targets and timing to improve long-term outcomes for these conduits.[16] This endeavor seeks to link dynamic gene networks to cell behavior and use this information to predict the time- and flow-dependent adaptations of the graft wall. Through a systematic deletion of the various elements that comprise this network, a series of virtual experiments can be used to examine the interconnectedness of the genes that regulate pathologic cell behaviors and identify the small set of genes that can be targeted to improve vein graft outcomes. Fundamental to such an undertaking is the seamless integration of large-scale experimental data sets with detailed mathematical models. The sequence of prediction and validation that occurs between these two approaches is an absolute requirement for a biologically and clinically useful multiscale modeling approach. The current evaluation of the time and flow dependent changes in cell proliferation in the hours to weeks following vein graft implantation is a key component of this effort. While publication is often focused on final conclusions, reporting experimental observations that are contained within these types of high resolution data sets, and the methodologies used to create them, is of substantial scientific benefit to other investigators in the field.
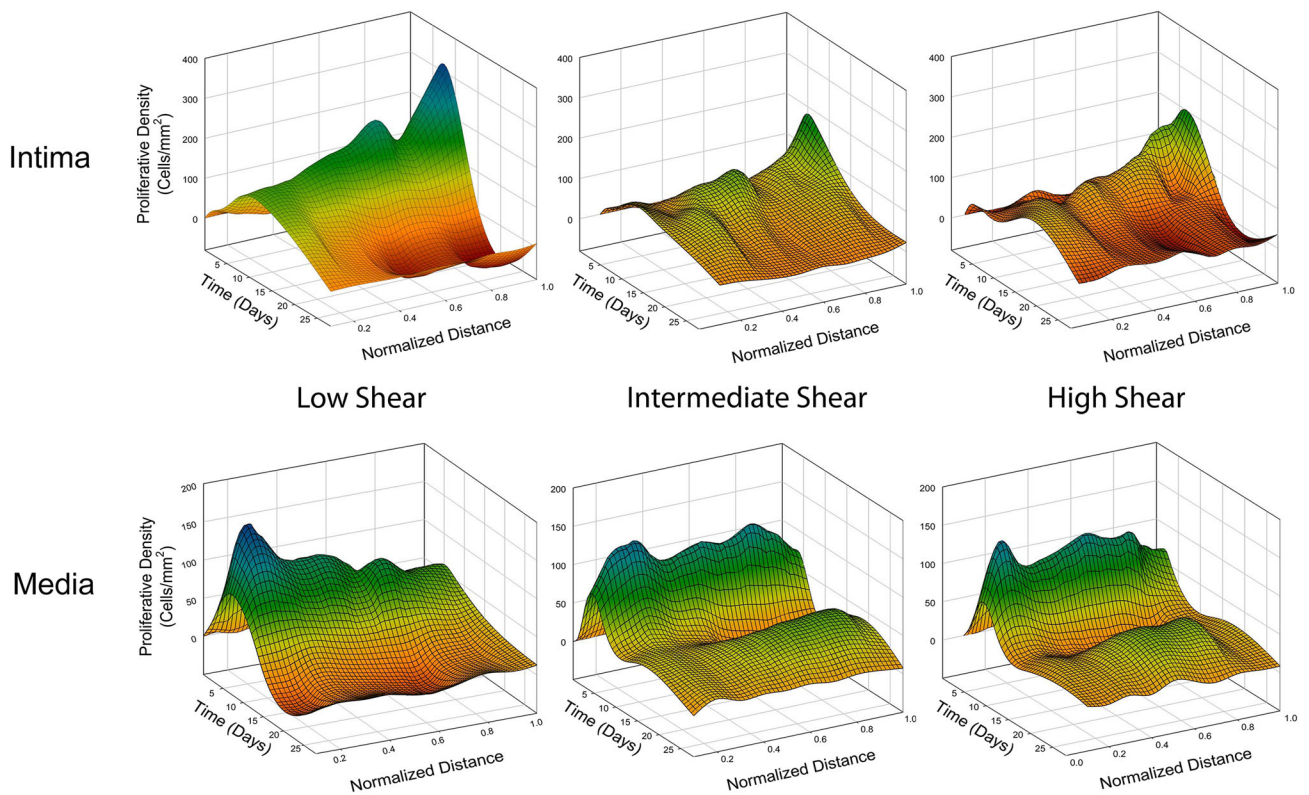
FIGURE 8. Spatial and temporal patterns of cell proliferation within the intima and media. To facilitate registration of the data, the intima and media for each graft specimen was virtually divided into 10 circumferential sections of equal thickness. For the intima, zero represents the section directly bordering the lumen, 0.5 represents the middle of the intima, and 1.0 represents the section bordering the IEL. For the media, zero represents the IEL, 0.5 represents the middle of the media, and 1.0 represents the section bordering the EEL. Note the peak in proliferative density in the intimal and medial regions that are adjacent to the IEL.
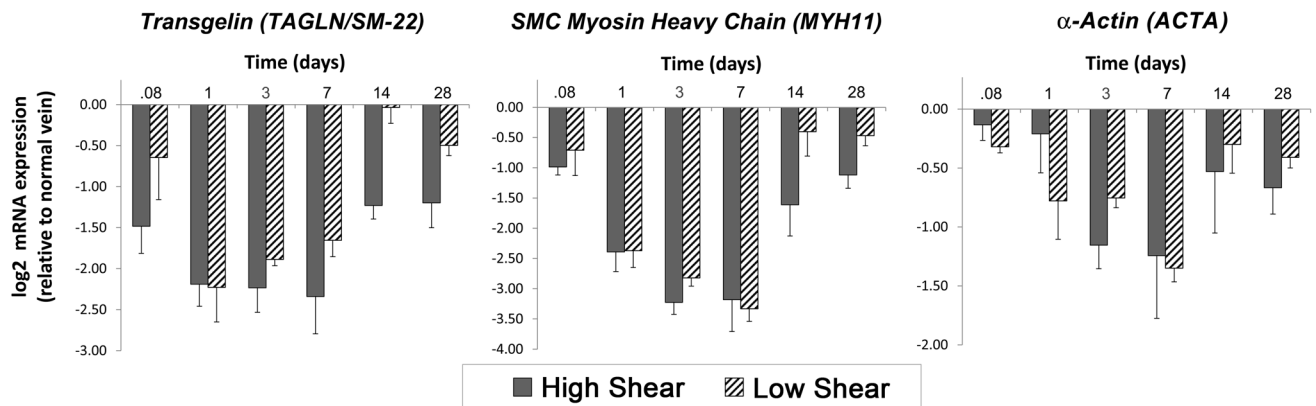

FIGURE 9. Within 2 h following graft implantation, there was a significant reduction in mRNA expression of the SMC contractile phenotype markers TAGLN ($p < .001$), MYH11 ($p < .001$), and ACTA ($p = .016$), which was seen to nadir at Day 7. TAGLN and MYH11 expression were also dependent on the imposed hemodynamics (TAGLN: $p < .001$, MYH11: $p < .035$), with a sustained decrease in expression under high flow conditions extending through 28 days.

Virtual Reconstruction Algorithm

A key component of the current analysis is the reconstruction methodology that translates a non-perfusion fixed histologic section to an *in vivo* architecture. Various reconstruction methodologies have previously described the rendering of a three-dimen-

sional image through use of consecutive histologic sections of a tissue.[1,3,5,18] In these examples, the final rendered image attempted to visually recreate the specimen as it was oriented after fixation and all other processing. While these methodologies provide a means for some analysis of the features of a tissue, they

are limited in their ability to provide insight into a tissue's interaction with its environment as well as the true spatial arrangement of markers at the cellular level. Little work has been done to recreate the effects of an *in vivo* environment on the deformation and orientation of a tissue, as was performed in the current study.

An area of increasing emphasis in scientific discovery is a systems-based understanding of biologic processes, where multiple high-resolution datasets are integrated to provide a multi-tiered understanding of the question at hand. Juxtaposed to this is the use of smaller, genetically modified *in vivo* models and limited human tissues. In line with these trends, our current methodology was developed to facilitate an integrated experimental-modeling approach, where multiple biologic measurements on each individual specimen are mandatory. In this series of experiments, high throughput genomics, histologic mapping of cell dynamics, immunohistochemical identification of the cell and matrix elements that comprise the wall, and extraction of morphologic geometries were performed on each harvested vein graft. An analysis that integrates these spatial scales with data obtained from each individual specimen is required to embrace the biologic complexity of the system. Harvesting techniques that provide such simultaneous, multi-faceted evaluations are required, and frequently negate the opportunity for aggressive fixation under physiologic conditions. The continued movement towards clinically-based experimentation, using patient derived tissues, presents a similar opportunity where the current reconstruction algorithms may be utilized.

Validation of the reconstruction algorithm predictions against non-invasive measurements of the *in vivo* graft geometry proved challenging due to the small diameter and relatively thin walls of the vein grafts. Conventional intravascular ultrasound devices (IVUS) offer an axial resolution of only 150–200 μm, which approximate the entire intima/media thickness of the graft. While commercially available optical coherence tomography (OCT) devices offer a 10-fold improvement in axial resolution (12–18 μm) the large diameter of the catheter relative to the rabbit inflow carotid artery limits the ability for intravascular placement. To circumvent these issues, a high-frequency ultrasound imaging system with the transducer placed external to the graft was utilized. With an axial resolution of 20 μm, validation was focused on the combined intima/media of grafts implanted for 28 days, where the measurement error using this technique could be minimized. While a distinct border between the intima and media was not well visualized using this technology, the blood/tissue interface and the loose connective tissue of the adventitia provided sufficient contrast for accurate measurements and an acceptable correlation with the predicted geometries.

One notable limitation of the current reconstruction algorithm relates to the ability to reconstruct histologic cross-sections with severely deformed, hairpin geometries. The nature of the inter-point distance algorithm is to measure the distance between a reference point on one boundary and its closest neighbor point on another boundary. In regions of severe deformity, the nearest point neighbor to a boundary reference point may no longer coincide with the next logical point moving along the adjacent boundary. For example, if the wall is folded upon itself such that there is a sharp bend extending into the lumen, identifying the closest neighbor lumen-IEL pairs fails to accurately track this region, resulting in a reconstruction that eliminates this hairpin deformity. In the current analysis, approximately 9% of the 190 samples demonstrated this degree of deformity and were excluded from the analysis.

Inherent to the generation of histologic cross-sections are variabilities in intimal or medial thickness that are artifacts of the processing methods. This propagates into the reconstruction algorithm as high frequency oscillations of the IEL or EEL interface. To approximate the *in vivo* geometries that were typically seen on ultrasound, this noise was mitigated in the final step of the reconstruction (Step 4, Fig. 3) by circularization of the IEL and EEL boundary lines while conserving the areas of the intima and media.

Temporal and Spatial Influence on Proliferation

The highest peak in intimal proliferation appeared at Day 7, during which the low flow grafts showed a significantly higher proliferative density than those from the intermediate and high flow conditions. Consistent with this increase in cell mass being a driver for intimal expansion, this peak precedes the time points at which the intimal area of the low flow grafts demonstrated rapid growth (Days 14 and 28).

Normalized cell distances provided an opportunity to compare the localization of proliferating cells within the graft, with particular emphasis on the boundaries of the intimal and medial compartments. The normalized distance data (Fig. 8, Supplemental Fig. 1) showed the highest proliferative density within the intima to be deep within this compartment, closest to the IEL. In contrast, the highest proliferative density in the media occurred in the superficial portion of this compartment, also adjacent to the IEL. While a variety of mechanisms may account for this pattern, it is interesting to speculate that the mechanical stress produced at this interface may be one of the primary drivers for this biology.

The intramural tensile stresses created by transposition of the vein to an arterial environment are propagated throughout the wall, with the distribution dependent on the mechanical properties of the tissue.[12,24] In the implanted vein graft, the IEL is the location where two layers with disparate elasticities are in direct contact.[13] This intersection causes the IEL to become the focal point of mechanical stress, which is dissipated into nearby cells.[20] Several studies have examined the effect of tensile forces on SMC behavior, demonstrating a close coupling between elevated tensile forces and enhanced cell replication.[11,28] This regional variation in the biomechanics at the interface may be the underlying mechanism for the observed distribution of proliferating cells.

In addition to altering the tensile stress distribution, the IEL may also be an important modulator of the local shearing forces caused by the flux of interstitial fluid through the wall. This fenestrated membrane, which circumscribes the vein graft, acts to channel flow into regions of discontinuity, resulting in significant regional variations in the interstitial fluid velocity.[29,30] Examined in an *in vitro* system, similar flow complexities have been shown to augment SMC replication rates, and may be a parallel mechanism for our observed proliferation pattern near the IEL.[2]

In conclusion, we have described an approach to extract the spatial distribution of proliferating cells within the intima and media of vein grafts following exposure to altered hemodynamic conditions. Through virtual reconstructions of unfixed, histologic specimens, the dynamic changes in cell proliferation and graft morphology were catalogued in the days to weeks following graft implantation. Such high resolution data sets are critical components of our systems-based understanding of vascular remodeling and key elements in our efforts to identify the genomic regulators of graft failure.

ELECTRONIC SUPPLEMENTARY MATERIAL

The online version of this article (doi:10.1007/s10439-016-1725-0) contains supplementary material, which is available to authorized users.

REFERENCES

[1]Arganda-Carreras, I., R. Fernandez-Gonzalez, A. Munoz-Barrutia, and C. Ortiz-De-Solorzano. 3D reconstruction of histological sections: application to mammary gland tissue. *Microsc. Res. Tech.* 73:1019–1029, 2010.

[2]Asada, H., J. Paszkowiak, D. Teso, K. Alvi, A. Thorisson, J. C. Frattini, F. A. Kudo, B. E. Sumpio, and A. Dardik. Sustained orbital shear stress stimulates smooth muscle cell proliferation via the extracellular signal-regulated protein kinase 1/2 pathway. *J. Vasc. Surg.* 42:772–780, 2005.

[3]Bagci, U., and L. Bai. Automatic best reference slice selection for smooth volume reconstruction of a mouse brain from histological images. *IEEE Trans. Med. Imaging* 29:1688–1696, 2010.

[4]Berceli, S. A., R. Tran-Son-Tay, M. Garbey, and Z. H. Jiang. Hemodynamically driven vein graft remodeling: a systems biology approach. *Vascular* 17:S2–S9, 2009.

[5]Cifor, A., T. Pridmore, and A. Pitiot. Smooth 3-D reconstruction for 2-D histological images. *Inf. Process Med. Imaging* 21:350–361, 2009.

[6]Conte, M. S., D. F. Bandyk, A. W. Clowes, G. L. Moneta, L. Seely, T. J. Lorenz, H. Namini, A. D. Hamdan, S. P. Roddy, M. Belkin, S. A. Berceli, R. J. DeMasi, R. H. Samson, and S. S. Berman. Results of PREVENT III: a multicenter, randomized trial of edifoligide for the prevention of vein graft failure in lower extremity bypass surgery. *J. Vasc. Surg.* 43:742–751, 2006.

[7]Dobrin, P. B., F. N. Littooy, and E. D. Endean. Mechanical factors predisposing to intimal hyperplasia and medial thickening in autogenous vein grafts. *Surgery* 105:393–400, 1989.

[8]Fernandez, C. M., D. R. Goldman, Z. Jiang, C. K. Ozaki, R. Tran-Son-Tay, and S. A. Berceli. Impact of shear stress on early vein graft remodeling: a biomechanical analysis. *Ann. Biomed. Eng.* 32:1484–1493, 2004.

[9]Garbey, M., and S. A. Berceli. A dynamical system that describes vein graft adaptation and failure. *J. Theor. Biol.* 336:209–220, 2013.

[10]Garratt, K. N., W. D. Edwards, U. P. Kaufmann, R. E. Vlietstra, and D. R. Holmes, Jr. Differential histopathology of primary atherosclerotic and restenotic lesions in coronary arteries and saphenous vein bypass grafts: analysis of tissue obtained from 73 patients by directional atherectomy. *J. Am. Coll. Cardiol.* 17:442–448, 1991.

[11]Haga, M., A. Yamashita, J. Paszkowiak, B. E. Sumpio, and A. Dardik. Oscillatory shear stress increases smooth muscle cell proliferation and Akt phosphorylation. *J. Vasc. Surg.* 37:1277–1284, 2003.

[12]Holzapfel, G. A., T. C. Gasser, and R. W. Ogden. A new constitutive framework for arterial wall mechanics and a comparative study of material models. *J. Elast.* 61:1–48, 2000.

[13]Holzapfel, G. A., G. Sommer, C. T. Gasser, and P. Regitnig. Determination of layer-specific mechanical properties of human coronary arteries with nonatherosclerotic intimal thickening and related constitutive modeling. *Am. J. Physiol. Heart Circ. Physiol.* 289:H2048–H2058, 2005.

[14]Hwang, M., S. A. Berceli, M. Garbey, N. H. Kim, and R. Tran-Son-Tay. The dynamics of vein graft remodeling induced by hemodynamic forces: a mathematical model. *Biomech. Model. Mechanobiol.* 11:411–423, 2012.

[15]Hwang, M., M. Garbey, S. A. Berceli, and R. Tran-Son-Tay. Rule-based simulation of multi-cellular biological

systems—a review of modeling techniques. *Cell. Mol. Bioeng.* 2:285–294, 2009.

[16]Hwang, M., M. Garbey, S. A. Berceli, R. L. Wu, Z. H. Jiang, and R. Tran-Son-Tay. Rule-based model of vein graft remodeling. *Plos One* 8:e57822, 2013.

[17]Jiang, Z., L. Wu, B. L. Miller, D. R. Goldman, C. M. Fernandez, Z. S. Abouhamze, C. K. Ozaki, and S. A. Berceli. A novel vein graft model: adaptation to differential flow environments. *Am. J. Physiol. Heart Circ. Physiol.* 286:H240–H245, 2004.

[18]Ju, T., J. Warren, J. Carson, M. Bello, I. Kakadiaris, W. Chiu, C. Thaller, and G. Eichele. 3D volume reconstruction of a mouse brain from histological sections using warp filtering. *J. Neurosci. Methods* 156:84–100, 2006.

[19]Kockx, M. M., B. A. Cambier, H. E. Bortier, G. R. De Meyer, and P. A. Van Cauwelaert. The modulation of smooth muscle cell phenotype is an early event in human aorto-coronary saphenous vein grafts. *Virchows Arch. A Pathol. Anat. Histopathol.* 420:155–162, 1992.

[20]Laurent, S., P. Boutouyrie, and P. Lacolley. Structural and genetic bases of arterial stiffness. *Hypertension* 45:1050–1055, 2005.

[21]Meyerson, S. L., C. L. Skelly, M. A. Curi, U. M. Shakur, J. E. Vosicky, S. Glagov, L. B. Schwartz, T. Christen, and G. Gabbiani. The effects of extremely low shear stress on cellular proliferation and neointimal thickening in the failing bypass graft. *J. Vasc. Surg.* 34:90–97, 2001.

[22]Owens, C. D., W. J. Gasper, A. S. Rahman, and M. S. Conte. Vein graft failure. *J. Vasc. Surg.* 61:203–216, 2015.

[23]Owens, G. K., M. S. Kumar, and B. R. Wamhoff. Molecular regulation of vascular smooth muscle cell differentiation in development and disease. *Physiol. Rev.* 84:767–801, 2004.

[24]Peterson, L. H., R. E. Jensen, and J. Parnell. Mechanical properties of arteries in vivo. *Circ. Res.* 8:622–639, 1960.

[25]Rzucidlo, E. M., K. A. Martin, and R. J. Powell. Regulation of vascular smooth muscle cell differentiation. *J. Vasc. Surg.* 45:25A–32A, 2007.

[26]Schwartz, L. B., M. K. O'Donohoe, C. M. Purut, E. M. Mikat, P. O. Hagen, and R. L. McCann. Myointimal thickening in experimental vein grafts is dependent on wall tension. *J. Vasc. Surg.* 15:176–186, 1992.

[27]Shi, Y., J. E. O'Brien, Jr, J. D. Mannion, R. C. Morrison, W. Chung, A. Fard, and A. Zalewski. Remodeling of autologous saphenous vein grafts. The role of perivascular myofibroblasts. *Circulation.* 95:2684–2693, 1997.

[28]Sumpio, B. E., A. J. Banes, L. G. Levin, and G. Johnson. Mechanical-stress stimulates aortic endothelial-cells to proliferate. *J. Vasc. Surg.* 6:252–256, 1987.

[29]Tada, S., and J. M. Tarbell. Interstitial flow through the internal elastic lamina affects shear stress on arterial smooth muscle cells. *Am. J. Physiol. Heart Circ. Physiol.* 278:H1589–H1597, 2000.

[30]Tada, S., and J. M. Tarbell. Flow through internal elastic lamina affects shear stress on smooth muscle cells (3D simulations). *Am. J. Physiol. Heart Circ. Physiol.* 282:H576–H584, 2002.

[31]Werner, M., A. Chott, A. Fabiano, and H. Battifora. Effect of formalin tissue fixation and processing on immunohistochemistry. *Am. J. Surg. Pathol.* 24:1016–1019, 2000.

[32]Zwolak, R. M., M. C. Adams, and A. W. Clowes. Kinetics of vein graft hyperplasia: association with tangential stress. *J. Vasc. Surg.* 5:126–136, 1987.